Available online at www.sciencedirect.com

ScienceDirect

IFAC Papers Online CONFERENCE PAPER ARCHIVE

IFAC PapersOnLine 50-1 (2017) 6989–6995

# Backstepping Control Method with Sliding Mode Observer for Autonomous Lane Keeping System

**Chang Mook Kang** * **Wonhee Kim** ** **Seung-Hi Lee** *
**Chung Choo Chung**† ***

* *Dept. of Electrical Engineering, Hanyang University, Seoul 04763, South Korea. (e-mail: kcm0728@hanyang.ac.kr, shlee@ieee.org).*
** *School of Energy Systems Engineering, Chung-Ang University, Seoul 06947, South Korea. (e-mail: whkim79@cau.ac.kr)*
*** *Div. of Electrical and Biomedical Engineering, Hanyang University, Seoul 04763, South Korea. (e-mail: cchung@hanyang.ac.kr), corresponding author*

**Abstract:** This study derived a novel reduced second-order model for an autonomous lane keeping system. The proposed reduced model of the lateral vehicle motion has the following two advantages: first, one can control the vehicle's lateral motion with only simple linear second-order dynamics and second, the state variable of the reduced model includes look-ahead distance likewise human driver. The backstepping control for the lateral control and the compensation of the system parameter and uncertainties is developed using the reduced model. Moreover, the reduced model-based sliding mode observer is designed to estimate the lateral velocity. The stability of the closed-loop system is proven using passivity. The lateral control performance of the proposed method is validated via numerical simulations using CarSim and MATLAB/Simulink and compared to the fourth-order lateral motion model-based linear quadratic controller.



*Keywords:* Vehicle model, Lateral control, Backstepping, Sliding mode observer, Stability.

- Nomenclature
  - $y$ : distance from center of gravity (c.g.) to the center of turn in ${}^{v}\{xyz\}$
  - $y_{des}$ : distance from the lane center to the center of turn in ${}^{v}\{xyz\}$
  - $e_y = y - y_{des}$ : lateral lane center offset at c.g.
  - $e_{yL} = y_L - y_{des,L}$ : lateral lane center offset at the look-ahead point
  - $L$ : look-ahead distance
  - $\psi_{des}$ : yaw angle slope of the lane center
  - $\psi_{des,L}$ : yaw angle slope of the lane center at the look-ahead point
  - $e_\psi = \psi_{des} - \psi$ : heading angle error at c.g.
  - $e_{\psi L} = \psi_{des,L} - \psi_L$ : heading angle error at the look-ahead point
  - $\dot{\psi}$ : yaw rate
  - $V$ : velocity of the vehicle at c.g.
  - $\alpha$ : tire slip angle
  - $\beta$ : side slip angle at c.g.
  - $C_\alpha$ : cornering stiffness of the tire
  - $F_y$ : lateral tire force
  - $I_z$ : yaw inertia of the vehicle
  - $m$ : total mass of the vehicle
  - $l$ : distance of the tire from c.g. of the vehicle
  - $u$ : input (=$\delta$ : steer angle) of the control system
- Subscripts
  - $f$ : front
  - $r$ : rear
  - $x$ : longitudinal
  - $y$ : lateral
  - $des$ : desired

## 1. INTRODUCTION

The control issues of autonomous vehicles for advanced drive assitant systems (ADASs) have been actively studied in the automotive industry. These ADASs and autonomous vehicles make driving safer and more convenient. The control issues of the ADASs and the autonomous vehicles can be classified into two types as follows: longitudinal and lateral controls. Many longitudinal control applications including adaptive cruise control and the autonomous emergency brake have been presented on the market. Meanwhile, the lateral control applications have not been developed as much as the longitudinal control applications because lateral control is closely related to vehicle stability. It is in this light that, only some adjuvant applications, which can be used by the driver to control the lateral position, have been released. These applications include the blind spot detection, lane keeping/change assistance and lane departure warning Navarro et al. (2011). The angle control method for the electric power steering system was recently developed for autonomous vehicles Kim et al. (2016).

Various lateral control methods for the lateral motion control, such as lane-keeping systems (LKSs) and lane change systems (LXSs), were studied to reach level 4 (high automation) and 5

⋆ †: Corresponding Author

This work was partly supported by Korea Evaluation Institute of Industrial Technology(KEIT) grant funded by the Korea government(MOTIE) (No.10044620, Automatic lane change system for novice drivers) and Institute for Information & communications Technology Promotion(IITP) grant funded by the Korea government(MSIP) (No.R7117-16-0164, Development of wide area driving environment awareness and cooperative driving technology which are based on V2X wireless communication).


10.1016/j.ifacol.2017.08.1341

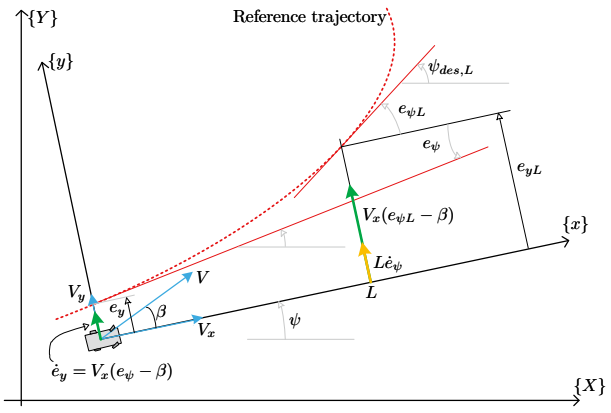


Fig. 1. Lateral motion with look-ahead distance

(full automation) defined in Society of Automotive Engineers (SAE) International Raksincharoensak et al. (2006); Navarro et al. (2011); Taylor et al. (1999); Hatipoglu et al. (2003); Chaib et al. (2004); Rossetter and Gerdes (2006); Wu et al. (2008); Naranjo et al. (2008); Son et al. (2015). A Lyapunov-based lateral control algorithm was proposed in Rossetter and Gerdes (2006) whereas a background control theory was presented for automated lane change maneuvers Hatipoglu et al. (2003). A lead-lag control method for the lateral motion was presented in Taylor et al. (1999). Moreover, a gain scheduling fuzzy control was proposed in Wu et al. (2008). A fuzzy controller that mimics human behavior and reactions during overtaking maneuvers was developed in Naranjo et al. (2008) Meanwhile, the performance of four lateral control methods was compared and studied in Chaib et al. (2004). A multi-rate lateral control scheme was recently proposed in Son et al. (2015); Kang et al. (2016a) to reduce the yaw rate ripple and lateral offset error. Lateral applications using a kinematic vehicle model were also proposed Kang et al. (2014a,b, 2016b). Although the previously mentioned methods improved the lateral control performance, the system and modeling uncertainties were not considered. In fact, measuring the lateral velocity is difficult even though it was assumed available for the controller in almost previous methods mentioned.

A backstepping control method with a sliding mode observer is presented in this paper for an autonomous lane keeping system. The reduced second-order model is proposed for the backstepping control design of the lateral dynamics. The backstepping control is developed for the lateral control and the compensation of the system and parameter uncertainties. The lateral position error is analyzed to converge to zero via the backstepping control. The sliding mode observer is designed to estimate the lateral velocity and the closed-loop system stability is proven using passivity. The lateral control performance of the proposed method is validated using CarSim and MATLAB/Simulink.

## 2. VEHICLE LATERAL MOTION MODEL

Figure 1 illustrates the lateral motion for the lane keeping system. We derive the model in terms of the lateral position and the velocity errors with respect to the road. The vehicle dynamic model is briefly described in the sections that follow.

### *2.1 Novel lateral motion model*

A generalized lateral dynamic motion model of a vehicle is considered herein. The lateral dynamic model consists of lateral position and yaw angle errors with respect to the road Rajamani (2011). The dynamic model can be described as follows in terms of the state vector $\mathbf{x} = [e_y \ \dot{e}_y \ e_\psi \ e_{\dot{\psi}}]^T$, control input $u = \delta$, and external signals $\varphi_d = [\dot{\psi}_{des}]^T$:

$$\dot{\mathbf{x}} = A\mathbf{x} + Bu + B_\varphi \varphi_d \tag{1}$$

where,

$$A = \begin{bmatrix} 0 & 1 & 0 & 0 \\ 0 & a_{22} & a_{23} & a_{24} \\ 0 & 0 & 0 & 1 \\ 0 & a_{42} & a_{43} & a_{44} \end{bmatrix}, \ B = \begin{bmatrix} 0 \\ b_{21} \\ 0 \\ b_{41} \end{bmatrix}, \ B_\varphi = \begin{bmatrix} 0 \\ a_{24} - V_x \\ 0 \\ a_{44} \end{bmatrix}$$

with

$$a_{22} = -\frac{2(C_{\alpha f} + C_{\alpha r})}{mV_x}, \quad a_{23} = -a_{22}V_x,$$

$$a_{24} = -1 - \frac{2(C_{\alpha f} l_f - C_{\alpha r} l_r)}{mV_x^2},$$

$$a_{42} = -\frac{2(C_{\alpha f} l_f - C_{\alpha r} l_r)}{I_z},$$

$$a_{43} = -a_{42}, \quad a_{44} = -\frac{2(C_{\alpha f} l_f^2 + C_{\alpha r} l_r^2)}{I_z V_x},$$

$$b_{21} = \frac{2C_{\alpha f}}{mV_x}, \quad b_{41} = \frac{2C_{\alpha f} l_f}{I_z}.$$

The lateral offset at the look-ahead distance, $L$, is represented as follows with clothoidal constraints in the third-order cubic polynomial Kang et al. (2014a,b):

$$e_{yL} = e_y + e_\psi L + \frac{\kappa}{2}L^2 + \frac{1}{6V_x}\frac{d\dot{\psi}}{dx}L^3. \tag{2}$$

We can approximate the third-order curved lane as a straight lane for either a small curvature or a small look-ahead distance. The lateral offset as the look-ahead distance (2) can then be approximated as follows:

$$\begin{aligned} e_{yL} &\approx e_y + e_\psi L \\ &= x_1 + Lx_3. \end{aligned} \tag{3}$$

Let us now define the new state $\mathbf{z}$ as follows to make use of the approximated $e_{yL}$

$$\begin{aligned} z_1 &= x_1 + Lx_3 \\ z_2 &= \dot{x}_1 + L\dot{x}_3 = x_2 + Lx_4. \end{aligned} \tag{4}$$

We obtain the dynamic of $z_2$ with constant velocity from Eqs. (1) and (4) as:

$$
\begin{aligned}
\dot{z}_2 &= \dot{x}_2 + L\dot{x}_4 \\
&= a_{22}x_2 + a_{23}x_3 + a_{24}x_4 + b_{21}u + (a_{24} - V_x)\dot{\psi}_{des} \\
&\quad + La_{42}x_2 + La_{43}x_3 + La_{44}x_4 + Lb_{41}u + La_{44}\dot{\psi}_{des} \\
&= (a_{22} + La_{42})x_2 + (a_{23} + La_{43})x_3 + (a_{24} + La_{44})x_4 \\
&\quad + (b_{21} + Lb_{41})u + (a_{24} + La_{44} - V_x)\dot{\psi}_{des} \\
&= (a_{22} + La_{42})x_2 + (a_{22} + La_{42})Lx_4 - (a_{22} + La_{42})Lx_4 \\
&\quad + (a_{24} + La_{44})x_4 + (a_{23} + La_{43})x_3 + \frac{(a_{23} + La_{43})}{L}x_1 \\
&\quad - \frac{(a_{23} + La_{43})}{L}x_1 + (b_{21} + Lb_{41})u + (a_{24} + La_{44} - V_x)\dot{\psi}_{des} \\
&= \underbrace{\frac{(a_{23} + La_{43})}{L}}_{\xi_1} z_1 + \underbrace{(a_{22} + La_{42})}_{\xi_2} z_2 - \underbrace{\frac{(a_{23} + La_{43})}{L}}_{\chi_1} x_1 \\
&\quad + \underbrace{(a_{24} + La_{44} - La_{22} - L^2 a_{42})}_{\chi_4} x_4 + (b_{21} + Lb_{41})u \\
&\quad + (a_{24} + La_{44} - V_x)\dot{\psi}_{des} \\
&= f + gu + h\dot{\psi}_{des}
\end{aligned}
\tag{5}
$$

where

$$
\begin{aligned}
f &= \xi_1 z_1 + \xi_2 z_2 - \chi_1 x_1 + \chi_4 x_4 \\
g &= b_{21} + Lb_{41} \\
h &= a_{24} + La_{44} - V_x.
\end{aligned}
$$

Consequently, the normal-form reduced second-order model (Eq. (6)) for the lateral control becomes:

$$
\begin{aligned}
\dot{z}_1 &= z_2 \\
\dot{z}_2 &= f + gu + h\dot{\psi}_{des}.
\end{aligned}
\tag{6}
$$

The reduced second order model (6) is in the form of the normal form. Thus, the system function and the parameter are in only $z_2$ dynamics.

### 2.2 Controller design via backstepping approach

The controller for the reduced-second order model (Eq. (6)) is developed in this subsection via the backstepping procedure. We define the tracking error $e = [e_1\ e_2]^T$ as follows:

$$
e_i = z_i - z_{i_d}. \tag{7}
$$

The tracking error dynamics is presented as follows:

$$
\begin{aligned}
\dot{e}_1 &= e_2 + z_{2_d} - \dot{z}_{1_d} \\
\dot{e}_2 &= f + gu - \dot{z}_{2_d}.
\end{aligned}
\tag{8}
$$

**Proposition 1.** Consider the tracking error dynamics (Eq. (8)). If the controller is designed by

$$
\begin{aligned}
z_{2_d} &= -k_1 e_1 + \dot{z}_{1_d} \\
u &= \frac{1}{g_o}\{-k_2 e_2 - f + \dot{z}_{2_d} - k_s \mathrm{sgn}(e_2)\}
\end{aligned}
\tag{9}
$$

where $k_1$, $k_2$ and $k_s$ are positive constants, then the origin of the tracking error dynamics (Eq. (8)) is exponentially stable. ◇

**Proof:** With the control law (Eq. (9)), the tracking error dynamics (Eq. (8)) becomes

$$
\begin{aligned}
\dot{e}_1 &= -k_1 e_1 + e_2 \\
\dot{e}_2 &= -k_2 e_2 - k_s \mathrm{sgn}(e_2).
\end{aligned}
\tag{10}
$$

A Lyapunov candidate function $V_{e_2}$ for stability analysis is defined as follows:

$$
V_{e_2} = \frac{1}{2}e_2^2 \tag{11}
$$

Differentiating $V_{e_2}$ with respect to time yields:

$$
\begin{aligned}
\dot{V}_{e_2} &= e_2\dot{e}_2 \\
&= e_2\left(-k_2 e_2 - k_s \mathrm{sgn}(e_2)\right) \\
&= -k_2 e_2^2 - k_s e_2 \mathrm{sgn}(e_2) \\
&\le -k_2 e_2^2 - k_s |e_2|.
\end{aligned}
\tag{12}
$$

Then, going one step ahead provides $V_{e_1}$ as follows:

$$
V_{e_1} = \frac{1}{2}e_1^2 \tag{13}
$$

Differentiating $V_{e_1}$ with respect to time yields:

$$
\begin{aligned}
\dot{V}_{e_1} &= e_1\dot{e}_1 \\
&= e_1\left(-k_1 e_1 + e_2\right) \\
&= -k_1 e_1^2 - k_1 e_1 e_2.
\end{aligned}
\tag{14}
$$

Equation (14) can be rewritten as follows if we define $e_2$ as the input and $e_1$ as the output in Eq. (8):

$$
k_1 \underbrace{e_1}_{output}\underbrace{e_2}_{input} = \dot{V}_{e_1} + \underbrace{k_1 e_1^2}_{>0}. \tag{15}
$$

Equation (15) shows that the relationship between $e_1$ and $e_2$ is strictly output passive Khalil (1996). In addition, $e_1$ is zero state observable. Therefore, the origin of the tracking error dynamics (Eq. (8)) is exponentially stable. ■

**Remark 1.** In the controller (Eq. (9)), $\mathrm{sgn}(e_2)$ is used for the robustness of the model and the parameter uncertainty. All state variables in most actual systems are physically bounded. Thus the parameter and system uncertainties are bounded Kosut (1983). The parameter and system uncertainties can be compensated if the control gain $k_s$ is large enough to suppress the parameter and system uncertainties. ◇

**Assumption 1.** In general highway driving situations, such as lane keeping, the ADASs are designed to keep the riding comfort of the driver and satisfy the stability of the vehicle motion. Thus, an upper bound $\beta_{max}$ such as $|\beta| \le \beta_{max}$ exists. The lateral acceleration of the vehicle is also very small. ◇

**Lemma 1.** Both the lateral offset $e_y = x_1$ and the heading angle error $e_\psi = x_3$ are regulated within small bounds if the approximated look-ahead distance $z_1$ exponentially converges to zero. ◇

**Proof:** We have obtain the following equation from the lateral vehicle dynamics Rajamani (2011) because $\dot{e}_y = \dot{y} + V_x e_\psi$:

$$
\dot{x}_1 = \dot{y} + V_x x_3. \tag{16}
$$

$z_1$ can then be represented by:

$$
\begin{aligned}
z_1 &= x_1 + Lx_3 \\
&= x_1 + \frac{L}{V_x}\dot{x}_1 - \frac{L\dot{y}}{V_x} \\
&= x_1 + \frac{L}{V_x}\dot{x}_1 - L\beta.
\end{aligned}
\tag{17}
$$

In Proposition 1, we showed that $z_1$ exponentially converges to zero. From Assumption 1, we see that we have $x_1 + \frac{L}{V_x}\dot{x}_1 - L\beta = 0$ in steady-state. Thus, $x_1$ converges to zero exponentially ultimately uniformly bounded. Consequently, $x_3$ also ultimately uniformly bounded. We see that $x_1$ and $x_3$ are regulated within small bounds because $\beta_{max}$ is small. ■

### 2.3 Sliding mode observer design

The observer is designed in this subsection to estimate the full state. Let us consider a system (Eq. (1)) with the following

measurement matrix:

$$C = \begin{bmatrix} 1 & 0 & 0 & 0 \\ 0 & 0 & 1 & 0 \\ 0 & 0 & 0 & 1 \end{bmatrix} \tag{18}$$

where $x_1 = e_y$ and $x_3 = e_\psi$ are measured from a lane detection vision sensor, and $x_4 = e_{\dot{\psi}}$ is measured from a vehicle motion sensor.

A state observer is also designed (Eq. (19)) as:

$$\dot{\hat{\mathbf{x}}} = A\hat{\mathbf{x}} + Bu - L_o\rho(CL_o)^{-1}\mathrm{sgn}(\hat{\mathbf{y}} - \mathbf{y}). \tag{19}$$

The system could be transformed into a canonical form as follows using a transformation matrix:

$$\begin{aligned} \dot{\bar{\mathbf{x}}} &= T_c\dot{\mathbf{x}} = T_cAT_c^{-1}T_c\mathbf{x} + T_cBu = \bar{A}\bar{\mathbf{x}} + \bar{B}u \\ \mathbf{y} &= CT_c^{-1}T_c\mathbf{x} = \bar{C}\bar{\mathbf{x}} \end{aligned} \tag{20}$$

where

$$T_c = \begin{bmatrix} \mathscr{N}^T(C) \\ C \end{bmatrix}, \ \bar{\mathbf{x}} = T_c\mathbf{x} = \begin{bmatrix} x_2 \\ \mathbf{y} \end{bmatrix}.$$

In the equation, $\mathscr{N}^T(C)$ denotes the null space of the measurement matrix. We find the following formulae when the canonical transformation matrix $T_c$ is applied to obtain a canonical form model:

$$\begin{aligned} -T_cL_o(CL_o)^{-1} &= -\begin{bmatrix} \mathscr{N}^T(C) \\ C \end{bmatrix} L_o(CL_o)^{-1} \\ &= \begin{bmatrix} -\mathscr{N}^T(C)L_o(CL_o)^{-1} \\ -I_p \end{bmatrix} = \begin{bmatrix} L_o \\ -I_p \end{bmatrix} \end{aligned}$$

and

$$\begin{aligned} \dot{\bar{\hat{\mathbf{x}}}} &= \bar{A}\bar{\hat{\mathbf{x}}} + \bar{B}u - T_cL_o\rho(CL_o)^{-1}\mathrm{sgn}(\hat{\mathbf{y}} - \mathbf{y}) \\ &= \bar{A}\bar{\hat{\mathbf{x}}} + \bar{B}u + \begin{bmatrix} L_o \\ -I_p \end{bmatrix} \rho\,\mathrm{sgn}(\hat{\mathbf{y}} - \mathbf{y}) \end{aligned} \tag{21}$$

$$\begin{cases} \dot{\hat{x}}_2 &= A_{11}\hat{x}_2 + A_{12}\hat{\mathbf{y}} + B_1u + L_o\rho\,\mathrm{sgn}(\hat{\mathbf{y}} - \mathbf{y}) \\ \dot{\hat{\mathbf{y}}} &= A_{21}\hat{x}_2 + A_{22}\hat{\mathbf{y}} + B_2u - \rho\,\mathrm{sgn}(\hat{\mathbf{y}} - \mathbf{y}). \end{cases}$$

where

$$\bar{A} = \begin{bmatrix} A_{11} & A_{12} \\ A_{21} & A_{22} \end{bmatrix}.$$

Let us now define:

$$\begin{aligned} \mathbf{e}_x &= \hat{\mathbf{x}} - \mathbf{x}, \\ \bar{\mathbf{e}}_x &= \hat{\mathbf{x}} - \bar{\mathbf{x}} = T_c\mathbf{e} = \begin{bmatrix} e_{x_2} \\ \mathbf{e}_y \end{bmatrix} = \begin{bmatrix} \hat{x}_2 - x_2 \\ \bar{\mathbf{y}} - \mathbf{y} \end{bmatrix}. \end{aligned} \tag{22}$$

Note that

$$\dot{\bar{\mathbf{e}}}_x = \bar{A}\bar{\mathbf{e}}_x + \begin{bmatrix} L_o \\ -I_p \end{bmatrix} \rho\,\mathrm{sgn}(\bar{C}\bar{\mathbf{e}}_x). \tag{23}$$

$$\begin{cases} \dot{e}_{x_2} &= A_{11}e_{x_2} + A_{12}\mathbf{e}_y + L_o\rho\,\mathrm{sgn}(\mathbf{e}_y) \\ \dot{\mathbf{e}}_y &= A_{21}e_{x_2} + A_{22}\mathbf{e}_y - \rho\,\mathrm{sgn}(\mathbf{e}_y). \end{cases}$$

The transformation matrix, $T_s$, is applied to make the discontinuous term appears at reaching mode:

$$T_s = \begin{bmatrix} I_{n-p} & L_o \\ 0 & I_p \end{bmatrix}$$

such that

$$\tilde{\mathbf{e}}_x = \begin{bmatrix} \tilde{e}_{x_2} \\ \tilde{\mathbf{e}}_y \end{bmatrix} = T_s\bar{\mathbf{e}}_x = T_s\begin{bmatrix} e_{x_2} \\ \mathbf{y} \end{bmatrix} = \begin{bmatrix} e_{x_2} + L_o\mathbf{e}_y \\ \mathbf{e}_y \end{bmatrix}$$

$$\begin{aligned} -T_s\begin{bmatrix} -L_o \\ I_p \end{bmatrix} \bar{C}\rho\,\mathrm{sgn}(\bar{\mathbf{e}}_x) &= -T_s\begin{bmatrix} -L_o \\ I_p \end{bmatrix} \rho\,\mathrm{sgn}(\mathbf{e}_y) \\ &= T_s\begin{bmatrix} L_o\rho\,\mathrm{sgn}(\mathbf{e}_y) \\ -\rho\,\mathrm{sgn}(\mathbf{e}_y) \end{bmatrix} = \begin{bmatrix} 0 \\ -\rho\,\mathrm{sgn}(\mathbf{e}_y) \end{bmatrix}. \end{aligned} \tag{24}$$

The error dynamics w.r.t. the new coordinates is obtained as follows:

$$\begin{aligned} \dot{\tilde{\mathbf{e}}}_x = T_s\dot{\bar{\mathbf{e}}}_x &= T_s\bar{A}T_s^{-1}T_s\bar{\mathbf{e}}_x - T_s\begin{bmatrix} -L_o \\ I_p \end{bmatrix} \bar{C}\rho\,\mathrm{sgn}(\bar{\mathbf{e}}_x) \\ &= \tilde{A}\tilde{\mathbf{e}}_x - \begin{bmatrix} 0 \\ \rho\,\mathrm{sgn}(\mathbf{e}_y) \end{bmatrix} \end{aligned} \tag{25}$$

$$\begin{cases} \dot{\tilde{e}}_{x_2} &= \tilde{A}_{11}\tilde{e}_{x_2} + \tilde{A}_{12}\mathbf{e}_y \\ \dot{\mathbf{e}}_y &= \tilde{A}_{21}\tilde{e}_{x_2} + \tilde{A}_{22}\mathbf{e}_y - \rho\,\mathrm{sgn}(\mathbf{e}_y) \end{cases}$$

where

$$\begin{aligned} \tilde{A} &= \begin{bmatrix} \tilde{A}_{11} & \tilde{A}_{12} \\ \tilde{A}_{21} & \tilde{A}_{22} \end{bmatrix}, \\ \tilde{A}_{11} &= A_{11} + L_oA_{21},\ \tilde{A}_{12} = A_{12} + L_oA_{22} - \tilde{A}_{11}L_o, \\ \tilde{A}_{21} &= A_{21},\ \tilde{A}_{22} = A_{22} + A_{21}L_o. \end{aligned}$$

Note that $s = C\mathbf{e}_x = CT_c^{-1}T_c\mathbf{e}_x = \bar{C}\bar{\mathbf{e}}_x = \mathbf{e}_y$ for the sliding mode. An objective of the observer is that $\tilde{e}_{x_2} \to 0$ as on the surface $\mathbf{e}_y = 0$ with the reachability condition $\mathbf{e}_y^T\dot{\mathbf{e}}_y < 0$ being satisfied.

**Proposition 2.** Consider the dynamics of $\tilde{e}_x$ (Eq. (25)). We have the following equation on the sliding surface:

$$\dot{\tilde{e}}_{x_2} = \tilde{A}_{11}\tilde{e}_{x_2} = (A_{11} + L_oA_{21})\tilde{e}_{x_2}. \tag{26}$$

$L_o$ is then determined such that $\lambda(A_{11} + L_oA_{21}) \in \mathbb{C}_-$.

The error system for the reaching mode becomes the following equation with a linear output error feedback:

$$\dot{\tilde{\mathbf{e}}} = \tilde{A}\tilde{\mathbf{e}} - F\mathbf{e}_y - \begin{bmatrix} 0 \\ \rho\,\mathrm{sgn}(\mathbf{e}_y) \end{bmatrix} \tag{27}$$

$$\begin{cases} \dot{\tilde{e}}_{x_2} &= \tilde{A}_{11}\tilde{e}_{x_2} + \tilde{A}_{12}\mathbf{e}_y - F_1\mathbf{e}_y \\ \dot{\mathbf{e}}_y &= \tilde{A}_{21}\tilde{e}_{x_2} + \tilde{A}_{22}\mathbf{e}_y - F_2\mathbf{e}_y - \rho\,\mathrm{sgn}(\mathbf{e}_y) \end{cases}$$

Choosing $F_1 = \tilde{A}_{12}$ and $F_2 = \tilde{A}_{22} + W_o$ with $W_o > 0$ leads to

$$\dot{\tilde{\mathbf{e}}}_x = \begin{bmatrix} \tilde{A}_{11} & 0 \\ \tilde{A}_{21} & -W_o \end{bmatrix} \tilde{\mathbf{e}}_x - \begin{bmatrix} 0 \\ \rho\,\mathrm{sgn}(\mathbf{e}_y) \end{bmatrix} \tag{28}$$

$$\begin{cases} \dot{\tilde{e}}_{x_2} &= \tilde{A}_{11}\tilde{e}_{x_2} \\ \dot{\mathbf{e}}_y &= \tilde{A}_{21}\tilde{e}_{x_2} - W_o\mathbf{e}_y - \rho\,\mathrm{sgn}(\mathbf{e}_y). \end{cases}$$

and, $W_o$ and $\rho$ are determined s.t. $e_y \to 0$ as $t \to \infty$. ◇

**Proof:** A Lyapunov candidate function $V_{\tilde{e}_{x_2}}$ for the stability analysis is defined as follows:

$$V_{\tilde{e}_{x_2}} = \frac{1}{2}\tilde{e}_{x_2}^2 \tag{29}$$

Differentiating $V_{\tilde{e}_{x_2}}$ with respect to time yields:

$$\begin{aligned} \dot{V}_{\tilde{e}_{x_2}} &= \tilde{e}_{x_2}\dot{\tilde{e}}_{x_2} \\ &= \tilde{A}_{11}\tilde{e}_{x_2}^2 \end{aligned} \tag{30}$$

A Lyapunov candidate function $V_{e_y}$ for the stability analysis is defined as follows:

$$V_{e_y} = \frac{1}{2}\mathbf{e}_y^T\mathbf{e}_y \tag{31}$$

Differentiating $V_{e_y}$ with respect to time yields:

$$\begin{aligned} \dot{V}_{e_y} &= \mathbf{e}_y^T\dot{\mathbf{e}}_y \\ &= \mathbf{e}_y^T\left(\tilde{A}_{21}\tilde{e}_{x_2} - W_o\mathbf{e}_y - \rho\,\mathrm{sgn}(\mathbf{e}_y)\right) \\ &= \mathbf{e}_y^T\tilde{A}_{21}\tilde{e}_{x_2} - \mathbf{e}_y^TW_o\mathbf{e}_y - \rho\mathbf{e}_y^T\,\mathrm{sgn}(\mathbf{e}_y) \end{aligned} \tag{32}$$

Equation (32) can be rewritten as follows if we define $\tilde{e}_{x_2}$ as the input and $\mathbf{e}_y$ as the output in Eq. (28):

$$\underbrace{\mathbf{e}_y^T}_{output}\underbrace{\tilde{A}_{21}\tilde{e}_{x_2}}_{input} = \dot{V}_{e_y} + \underbrace{\mathbf{e}_y^T W_o \mathbf{e}_y + \rho \mathbf{e}_y^T \mathrm{sgn}(\mathbf{e}_y)}_{>0}. \tag{33}$$

Equation (33) shows that the relationship between $\mathbf{e}_y$ and $\tilde{e}_{x_2}$ is strictly output passive Khalil (1996). In addition, $\tilde{e}_{x_2}$ is zero state observable. Therefore, the origin of the error dynamics (Eq. (28)) is exponentially stable. ■

### 2.4 Closed-loop system stability

In practice, measuring $e_2$ is difficult. Thus, instead of $e_2$, $\hat{e}_2$ is used in the controller (Eq. (9)). The error dynamics (Eq.(10)) is thn changed into

$$\begin{aligned} \dot{e}_1 &= -k_1 e_1 + e_2 \\ \dot{e}_2 &= -k_2 e_2 - k_s \mathrm{sgn}(e_2) + k_2 \tilde{e}_2 + k_s f(e_2, \hat{e}_2). \end{aligned} \tag{34}$$

where $f(e_2, \hat{e}_2) = \mathrm{sgn}(e_2) - \mathrm{sgn}(\hat{e}_2)$. The closed-loop system can be presented as follows from Eqs. (35) and (28)

$$\begin{aligned} \dot{e}_1 &= -k_1 e_1 + e_2 \\ \dot{e}_2 &= -k_2 e_2 - k_s \mathrm{sgn}(e_2) + k_2 \tilde{e}_2 + k_s f(e_2, \hat{e}_2) \\ \dot{\tilde{e}}_{x_2} &= \tilde{A}_{11} \tilde{e}_{x_2} \\ \dot{\tilde{\mathbf{e}}}_y &= \tilde{A}_{21} \tilde{e}_{x_2} - W_o \mathbf{e}_y - \rho sgn(\mathbf{e}_y). \end{aligned} \tag{35}$$

$f(e_2, \hat{e}_2)$ is bounded in Eq. (35). Thus, the error dynamics (Eq. (10)) from $f(e_2, \hat{e}_2)$ to $e_1$ and $e_2$ are input-to-state (ISS) stable. The estimation errors $\tilde{e}_{x_2}$ and $\tilde{\mathbf{e}}_y$ are proven to converge to zeros. Thus, $f(e_2, \hat{e}_2)$ converges to zero as $\tilde{e}_{x_2}$ converges to zero s.t $\hat{z}_2 = \hat{x}_2 + Lx_4$. Consequently, both $e_1$ and $e_2$ converge to zeros.

## 3. APPLICATION RESULTS

The proposed method was validated via computational simulation results. In the simulation, CarSim and MATLAB/Simulink were implemented as the dynamic vehicle motion solver and for the controller and the observer, respectively. During the simulation, we set the vehicle speed as $80km/h$, and the vehicle traveled along the two following cases:

- Case1: Straight and circular road segments
- Case2: *S*-curved road satisfying the clothoidal constraints

The Parameters used in the simulation study were the nominal values of a small sports utility vehicle, the Tucson from HYUNDAI Motors. We could verify the effect of a look-ahead distance in the proposed backstepping approach controller under various look-ahead distances.

Figures 2 and 3 show the vehicle motion data and the performance of the proposed controller in Case1, respectively. Figure 2(c) presents the performance of the proposed sliding mode observer. The observer on constant curvature road had an offset error because the model used in Eq. (28) was approximately linearized for a small sideslip angle ($\tan\beta \approx \beta$). Nevertheless, we observed that the proposed method-based lane keeping system exhibited quite a reasonable performance with the lateral offset, $c_0$, within $0.01m$ on both the straight and constant curvature roads in Fig. 3(b). In practice, using a high gain $k_s$ of Eq.(9) is not desirable. The high value of $k_s$ causes chattering in the steering angle, thereby resulting in an uncomfortable yaw rate. However, $z_1$ began to converge to zero when the vehicle got into the straight lane road coming out of the circle road. We may add a disturbance observer to the backstepping controller to remove the such excessive chattering. The transient between

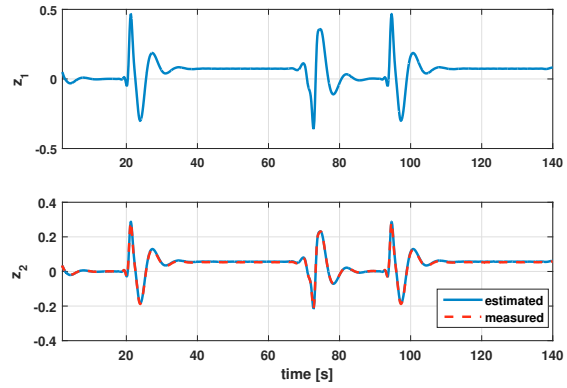


(a) $z_1 = x_1 + Lx_3$ and $z_2 = x_2 + Lx_4$.

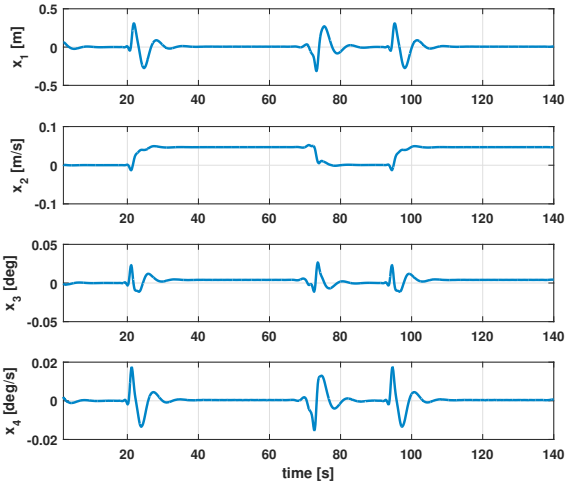


(b) States of the fourth-order lateral motion model with respect to the road.

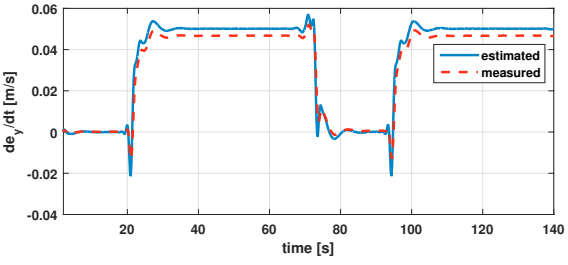


(c) $\hat{e}_y$ and $e_y$.

Fig. 2. Vehicle motion data. $\beta_m$ and $x_2$ are not directly measured from the vehicle sensor. We obtain the data from the vehicle dynamic motion solver, CarSim.

two segments did not satisfy the clothoidal constraints because the road segments in the Case 1 are straight and circular. Therefore, one may observe the ripple of the yaw rate and the steering wheel angle in Figs. 2 and 3, respectively. In practice, a highway is designed to meet the clothoidal constraints, such that an oscillation does not occur, as shown in Figs. 2 and 3.

Figure 4 shows the steering wheel angle with respect to the look-ahead distance $L$ used in the backstepping approach control. The transient responses are equivalent to the step responses to $\varphi_d$ when the vehicle gets into the circle road. The lateral motion control using the look-ahead distance $L$ actually determines $L$ according to the vehicle longitudinal velocity. This

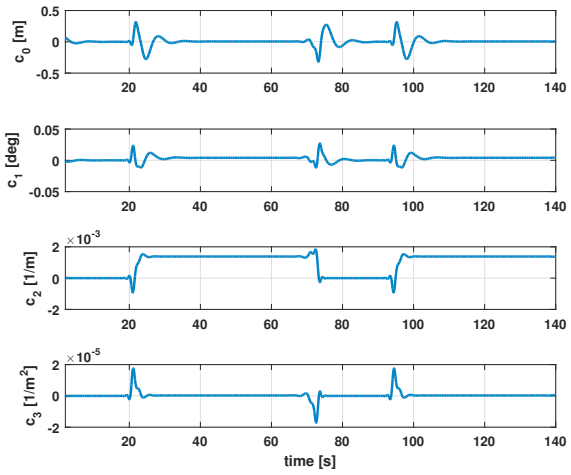


(a) Camera module data. $c_0$ denotes the lateral lane center offset at c.g.; $c_1$ denotes the in-lane heading slope and the heading angle error at c.g.; $c_2$ denotes curvature/2 at $s = 0$; and $c_3$ denotes the curvature-rate/6.

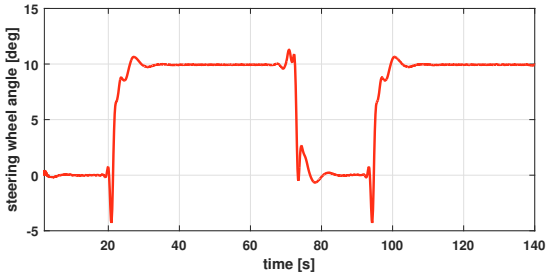


(b) Steering wheel angle.

Fig. 3. Lane keeping performance and steering wheel angle of the proposed method.

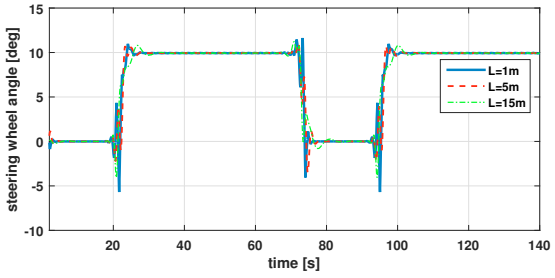


(a) Steering wheel angle.

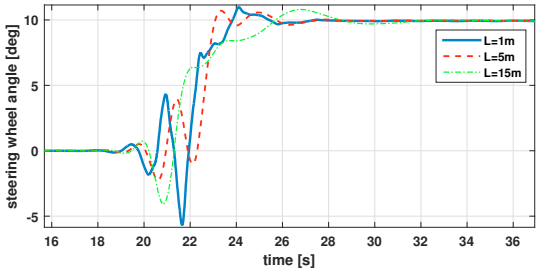


(b) Enlarged steering wheel angle.

Fig. 4. Steering wheel angle tracking performance of the proposed method without the driver torque disturbance.

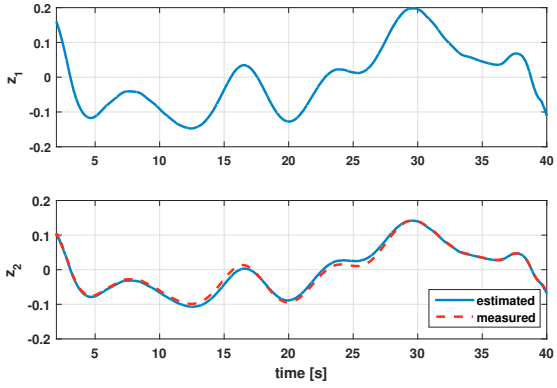


(a) $z_1 = x_1 + Lx_3$ and $z_2 = x_2 + Lx_4$.

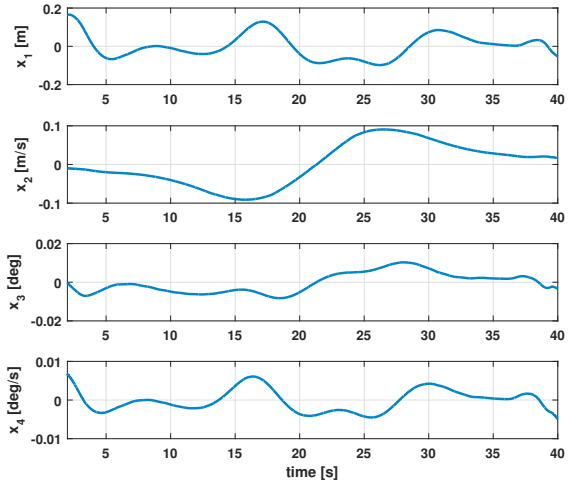


(b) States of the fourth-order lateral motion model with respect to the road.

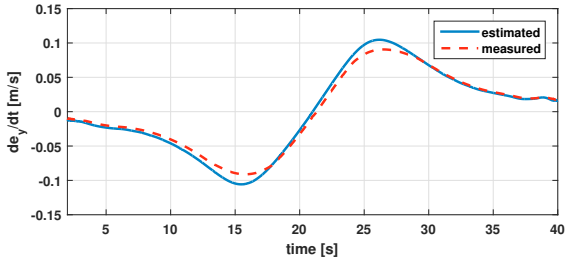


(c) $\hat{e}_y$ and $e_y$.

Fig. 5. Vehicle motion data. $\beta_m$ and $x_2$ are not directly measured from the vehicle sensor. We obtain the data from the vehicle dynamic motion solver, CarSim.

variation of $L$ affects the locations of the system zeros such that the damping ratio of the dominant poles is influenced Son et al. (2015). $L$ is close to the front of the vehicle. Hence, the damping ratio of the poles drastically declines. Figure 4 also illustrates the damping effect of the look-ahead distance in the proposed method.

Figures 5 and 6 show the vehicle motion data and the performance of the proposed controller in Case 2, respectively. Figure 5(c) presents the performance of the proposed sliding mode observer. The offset error of the sliding mode observer became larger as the curvature increased because we used an

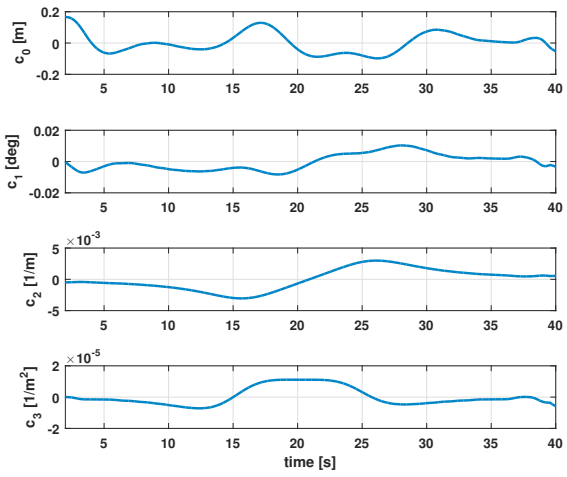


(a) Camera module data. $c_0$ denotes the lateral lane center offset at c.g.; $c_1$ denotes the in-lane heading slope and the heading angle error at c.g.; $c_2$ denotes curvature/2 at $s = 0$; $c_3$ denotes the curvature-rate/6.

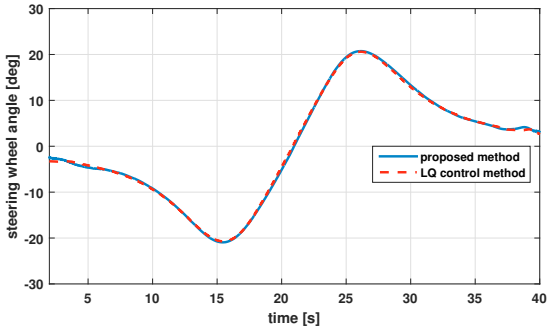


(b) Steering wheel angle, the presented linear quadratic (LQ) control method is described in Son et al. (2015).

Fig. 6. Lane keeping performance and steering wheel angle of the proposed method on road satisfying clothoidal constraints.

approximately linearized sideslip angle ($\tan\beta \approx \beta$). Although an offset error existed in the observer, the proposed method showed a quite reasonable performance compared to the linear quadratic (LQ) control method described in Son et al. (2015). The proposed method performed lane keeping within $0.1m$ on the curved road satisfying the clothoidal constraints in Fig. 6(b).

## 4. CONCLUSION

This study derived a novel reduced second-order model for an autonomous lane keeping system. A backstepping controller and a sliding mode observer were designed to control the lateral motion and estimate the lateral velocity, respectively. We found that the reduced second-order model-based lateral motion controller showed a reasonable performance compared to fourth-order lateral motion model-based controller that regulated the lateral offset at the look-ahead distance. Moreover, the experimental results showed that the reduced model could reflect the damping effect of the look-ahead distance. The validations of the backstepping controller and the sliding mode observer under various driving conditions and environments will be discussed in future works. In addition, a hardware-in-the-loop system and a test vehicle-based validation will be analyzed.

## REFERENCES


Chaib, S., Netto, M.S., and Mammar, S. (2004). H, adaptive, pid and fuzzy control: a comparison of controllers for vehicle lane keeping. In *IEEE intelligent vehicles symposium*, 139–144.

Hatipoglu, C., Ozguner, U., and Redmill, K.A. (2003). Automated lane change controller design. *IEEE transactions on intelligent transportation systems*, 4(1), 13–22.

Kang, C.M., Gu, Y.S., Jeon, S.J., Son, Y.S., Kim, W., Lee, S.H., and Chung, C.C. (2016a). Lateral control system for autonomous lane change system on highways. *SAE International Journal of Passenger Cars-Mechanical Systems*, 9(2016-01-1641), 877–884.

Kang, C.M., Lee, S.H., and Chung, C.C. (2014a). Comparative evaluation of dynamic and kinematic vehicle models. In *53rd IEEE Conference on Decision and Control*, 648–653.

Kang, C.M., Lee, S.H., and Chung, C.C. (2014b). Lane estimation using a vehicle kinematic lateral motion model under clothoidal road constraints. In *17th International IEEE Conference on Intelligent Transportation Systems*, 1066–1071.

Kang, C.M., Lee, S.H., and Chung, C.C. (2016b). Lane keeping system based on kinematic model with road friction coefficient adaptation. In *Intelligent Vehicles Symposium (IV), 2016 IEEE*, 552–557.

Khalil, H.K. (1996). *Nonlinear systems*, volume 3. Prentice hall New Jersey.

Kim, W., Son, Y.S., and Chung, C.C. (2016). Torque-overlay-based robust steering wheel angle control of electrical power steering for a lane-keeping system of automated vehicles. *IEEE Transactions on Vehicular Technology*, 65(6), 4379–4392.

Kosut, R. (1983). Design of linear systems with saturating linear control and bounded states. *IEEE Transactions on Automatic Control*, 28(1), 121–124.

Naranjo, J.E., Gonzalez, C., Garcia, R., and De Pedro, T. (2008). Lane-change fuzzy control in autonomous vehicles for the overtaking maneuver. *IEEE Transactions on Intelligent Transportation Systems*, 9(3), 438–450.

Navarro, J., Mars, F., and Young, M.S. (2011). Lateral control assistance in car driving: classification, review and future prospects. *IET Intelligent Transport Systems*, 5(3), 207–220.

Rajamani, R. (2011). *Vehicle dynamics and control*. Springer.

Raksincharoensak, P., Nagai, M., and Shino, M. (2006). Lane keeping control strategy with direct yaw moment control input by considering dynamics of electric vehicle. *Vehicle System Dynamics*, 44(sup1), 192–201.

Rossetter, E.J. and Gerdes, J.C. (2006). Lyapunov based performance guarantees for the potential field lane-keeping assistance system. *Journal of dynamic systems, measurement, and control*, 128(3), 510–522.

Son, Y.S., Kim, W., Lee, S.H., and Chung, C.C. (2015). Robust multirate control scheme with predictive virtual lanes for lane-keeping system of autonomous highway driving. *IEEE Transactions on Vehicular Technology*, 64(8), 3378–3391.

Taylor, C.J., Košecká, J., Blasi, R., and Malik, J. (1999). A comparative study of vision-based lateral control strategies for autonomous highway driving. *The International Journal of Robotics Research*, 18(5), 442–453.

Wu, S.J., Chiang, H.H., Perng, J.W., Chen, C.J., Wu, B.F., and Lee, T.T. (2008). The heterogeneous systems integration design and implementation for lane keeping on a vehicle. *IEEE Transactions on Intelligent Transportation Systems*, 9(2), 246–263.